



Evaluation of CLEAN-SC, B-CLEAN-SC, HR-CLEAN-SC, and Local Optimization for wind tunnel applications

Armin Goudarzi
German Aerospace Center (DLR)
Bunsenstr a e 10, 37073 G ttingen

Abstract

This paper presents a comparison of the methods CLEAN-SC, Broadband-CLEAN-SC, High-Resolution-CLEAN-SC, and Local Optimization. The methods are evaluated on increasingly complex data such as synthetic data, a generic open wind tunnel experiment, and the closed wind tunnel Do728 "DLR-1" case. The results show that CLEAN-SC produces stable results for all data with fast processing speed. HR-CLEAN-SC is able to halve the observable frequency but is slow and shows artifacts at high frequencies. B-CLEAN-SC is about 10x slower than CLEAN-SC but extends the observable frequency range greatly and suppresses noise. Local Optimization can be applied in low background noise situations to further improve spectral estimations but fails in high background noise scenarios. Reference Python implementations and data are available.

1 Introduction

For the localization and estimation of the sound power at complex source geometries, beamforming is well-established [20]. Each field of application in acoustical imaging has particular challenges. In aeroacoustic imaging, the number of sensors is typically favorably large compared to the number of observed sources [8]. The array's aperture is typically favorably large compared to the observed object and its distance in closed wind tunnel applications and reasonably large in open wind tunnel applications. However, the Signal-to-Noise Ratio (SNR) is unfavorably low in closed test sections (uncorrelated noise typically exceeds the signal by over 15 dB), so blind source separation methods and signal subspace-based methods fail for this application.

Most methods are grid-based so that focus points are predefined in the area of interest since they proved to be robust. Beamforming is then evaluated on these predefined points. Due to the increasing computational power, many algorithms are now evaluated on 3D problems to improve accuracy [2], where the number of focus points is typically vast compared to the number of microphones so that even a solution for radiating sources is no longer unique. Thus, various beamforming methods and algorithms emerged over the last decades to account for different use cases, configurations, and assumptions.

For closed wind tunnel applications, CLEAN-SC [23] is still the industry gold standard due to its robustness, the straightforward spatial integration of the results, and well-known limitations. These limitations comprise the handling of coherent, and distributed sources, as well as the wrong spatial and source power estimation at frequencies below the Rayleigh resolution limit and frequencies above the sensor spacing wavelength due to aliasing. Another inherent limitation is the use of normalized Green's functions, so-called steering vectors, which can only be either correct in the spatial source localization or the power estimation, but never both [5, 22].

Novel beamforming methods are continuously presented with theoretical benefits over conventional beamforming and CLEAN-SC. However, they are typically evaluated on simple, generic data to help understand their functionality, which in return makes it difficult to judge their behavior in complex environments such as noisy wind tunnels. Further, algorithmic implementation details are often crucial, but not included in the publications, and a reference code is not provided. As a result, potentially interesting, new methods are not applied in expensive industrial experiments where conservative clients favor well-explored, robust algorithms despite their limitations.

This paper explores the behavior of the CLEAN-SC extensions Broadband-CLEAN-SC [12] (B-CLEAN-SC), and HR-CLEAN-SC [24]. Further, a hybrid method using Local Optimization [14] (LO) based on an initial B-CLEAN-SC solution is presented. The methods are evaluated on synthetic, incoherent monopoles, on real monopole measurements using a speaker in an open wind tunnel, and on the "DLR-1" case [1, 3], featuring a Dornier 728 (Do728) model in a closed test section wind tunnel.

Reference implementations of CLEAN-SC, B-CLEAN-SC, HR-CLEAN-SC, and data are available in Python at GitHub [10]. The HR-CLEAN-SC implementation is based on the MatLab code by Gilles Chardon [6] at GitHub [4].

2 Theory

This section presents relevant theory concerning CLEAN-SC, B-CLEAN-SC, and Local optimization [14]. Source positions are denoted with y , receiver and sensor positions with x .

2.1 Cross Spectral Matrix

The Cross Spectral Matrix (CSM) corresponding to M sensors on the positions $\mathbf{x} = \vec{x}_1, \dots, \vec{x}_M$ is given by the complex microphone pressure vector \mathbf{p}

$$\mathbf{p} = [p(\vec{x}_1), \dots, p(\vec{x}_M)]^T \quad (1)$$

with

$$\mathbf{C} = \langle \mathbf{p}\mathbf{p}^\dagger \rangle \quad (2)$$

where \dagger denotes the Hermitian (conjugate transpose), and $\langle \dots \rangle$ the block averages. For a compact monopole without flow, the Green's matrix \mathbf{G} of size $\mathcal{C}^{(M \times N)}$ between the N source positions \mathbf{y} and M sensors \mathbf{x} is

$$\mathbf{G}(\mathbf{x}, \mathbf{y}) = \frac{\exp(-jk\mathbf{R})}{4\pi\mathbf{R}}, \quad (3)$$

where $\mathbf{R} = \|\mathbf{x} - \mathbf{y}\|_2$ (l_2 -norm) is a matrix of size $\mathcal{R}^{(M \times N)}$. Given the source matrix \mathbf{Q} , the CSM can be derived straight forward with

$$\mathbf{C} = \mathbf{G}\mathbf{Q}\mathbf{Q}^\dagger, \quad (4)$$

where incoherent energy is along the diagonal, and coherent energy at the corresponding cross-entries [11]. Coherent sources will be not further discussed in this paper, so that $\mathbf{Q} = \text{diag}(\mathbf{q})$ is a diagonal matrix, and $\mathbf{q} = q_1, \dots, q_N$. Then, eq. 4 is equivalent to

$$\mathbf{c} = \mathbf{T}\mathbf{q}, \quad (5)$$

where \mathbf{c} is the vectorized CSM, and \mathbf{T} is the propagation operator. The propagation operator \mathbf{T} is of size $\mathcal{C}^{(M^2 \times N)}$, and the vectorized CSM \mathbf{c} of dimension M^2 . The propagation operator is derived from the Green's Matrix \mathbf{G} with

$$\mathbf{T} = \mathbf{G} \odot \mathbf{G}^\dagger, \quad (6)$$

where \odot is the Khatri-Rao product [25], a column-wise Kronecker product.

2.2 Conventional beamforming

Conventional beamforming is a method to estimate the acoustic source radiation at a fixed focus grid, based on a source assumption, typically a monopole. [20]. The advantage of this method is its computational speed, since it is only comprised of matrix multiplications, and its robustness. Conventional beamforming estimates the source power by discretizing \mathbf{q} in eq. 4 and solving for it by rearranging the equation. Then, for each discretized source q' the estimated power is

$$q' = \mathbf{g}^\dagger \mathbf{C}\mathbf{g}. \quad (7)$$

Note, that the matrix multiplication on the right-hand side is a summation over all sensor combinations, that yields an arbitrary value. To obtain a meaningful value, the Green's function g is

normalized, which yields a so-called steering vector h , so that the beamforming result b is

$$b = \mathbf{w}^\dagger \mathbf{C} \mathbf{w}. \quad (8)$$

Four steering vectors w are typically regarded [5, 22].

$$\mathbf{w}^{\text{I}} = \frac{1}{M} \frac{\mathbf{g}}{|\mathbf{g}|} \quad (9)$$

$$\mathbf{w}^{\text{II}} = \frac{1}{M} \frac{\mathbf{g}}{|\mathbf{g}|^2} \quad (10)$$

$$\mathbf{w}^{\text{III}} = \frac{\mathbf{g}}{\|\mathbf{g}\|_2^2} \quad (11)$$

$$\mathbf{w}^{\text{IV}} = \frac{1}{\sqrt{M}} \frac{\mathbf{g}}{\|\mathbf{g}\|_2} \quad (12)$$

The desired property of a steering vector is that the beamforming map $\mathbf{b}(\mathbf{y})$ achieves the correct level at the true source location \mathbf{y}_S , so that

$$q(\mathbf{y}_S) = \mathbf{w}^\dagger(\mathbf{x}, \mathbf{y}_S) \mathbf{C}(\mathbf{x}) \mathbf{w}(\mathbf{x}, \mathbf{y}_S) = b(\mathbf{y}_S). \quad (13)$$

Additionally, the source location is desired to be correct so that the maximum level of the source map appears at the source location

$$\mathbf{b}(\mathbf{y} = \mathbf{y}_S) > \mathbf{b}(\mathbf{y} \neq \mathbf{y}_S). \quad (14)$$

Formulation I is normalized by the absolute value of the Green's function and, thus, only compensates the phase. While it satisfies the second condition [5, 22] based on its spatial derivatives at the true source position, the first condition is only met at a reference position \mathbf{y}_R , so that $d_S = |\mathbf{x} - \mathbf{y}_S|$, $d_R = |\mathbf{x} - \mathbf{y}_R|$

$$g(\mathbf{x}, \mathbf{y}_S, \mathbf{y}_R) = \frac{\exp(-jk(d_S - d_R))}{4\pi(d_S - d_R)}, \quad (15)$$

and thus

$$\mathbf{b}(\mathbf{y}_S) = \left(\frac{1}{M} \sum_{m=1}^M \frac{d_R}{d_S} \right)^2 q. \quad (16)$$

With an increasing distance $d = |\mathbf{y} - \mathbf{y}_R|$, the source power estimation error will increase. Formulation II additionally compensates for the Green's function's amplitude and thus meets condition one. Condition two is violated so that the maximum in the beamforming map does not reassemble the true source location. Formulation III is typically connected to "conventional beamforming" and can be interpreted as the Maximum Likelihood Estimator because its l_2 -norm normalization

$$\mathbf{A} = \frac{\mathbf{g}^\dagger \mathbf{C}}{\|\mathbf{g}\|^2} \quad (17)$$

minimizes the Mean Squared Error (MSE) between the observed CSM and the estimated source

power

$$\text{MSE} = |\mathbf{C} - \mathbf{A}\mathbf{g}|^2. \quad (18)$$

The MSE and the variance of Formulation III are smaller or equal compared to Formulation II [5]. Formulation IV seeks to minimize the MSE with $h^\dagger h = 1/N$, which satisfies condition two but only yields the power estimation

$$\mathbf{b}(\mathbf{y}_S) = \frac{1}{M} \sum_{m=1}^M \frac{d_R^2}{d_S^2} 2q, \quad (19)$$

of which the error is less or equal to formulation I [5]. Ernst [9] formalized the steering vector normalization with

$$w(\mathbf{y}) = \hat{w}(\mathbf{y}) \exp(j\varphi(\mathbf{y})) \quad (20)$$

and

$$\hat{w}(\mathbf{y}) = \frac{|g(\mathbf{y})|^{\beta-1}}{(\sum_m^M |g_m(\mathbf{y})|^\beta)^\alpha} \quad (21)$$

that satisfies condition one for $\alpha = 1, \beta \in \mathbb{R}$, and condition two for $\alpha = 1 - 1/\beta$. Both conditions can only be met at $\beta \rightarrow \infty$, where beamforming renders useless due to the weighting of the microphones. With

$$\angle w = \frac{w}{|w|} \quad (22)$$

the steering vectors result from eq. 21 with

$$\mathbf{w}^I \quad \alpha = 0 \quad \beta = 1 \quad \hat{\mathbf{w}} = \frac{1}{M} \quad (23)$$

$$\mathbf{w}^{II} \quad \alpha = 1 \quad \beta = 0 \quad \hat{\mathbf{w}} = \frac{1}{M} \frac{1}{|\mathbf{g}|} \quad (24)$$

$$\mathbf{w}^{III} \quad \alpha = 1 \quad \beta = 2 \quad \hat{\mathbf{w}} = \frac{|\mathbf{g}|}{\|\mathbf{g}\|_2^2} \quad (25)$$

$$\mathbf{w}^{IV} \quad \alpha = \frac{1}{2} \quad \beta = 1 \quad \hat{\mathbf{w}} = \frac{1}{\sqrt{M}} \frac{|\mathbf{g}|}{\|\mathbf{g}\|_2} \quad (26)$$

Eq. 21 shows that it is impossible to obtain a steering vector, that yields both of the desired properties at the same time, which is the inherent limitation of conventional beamforming, and its derivative methods such as CLEAN-SC.

Conventional beamforming yields an estimation of the source radiation for each chosen focus point \mathbf{y} . This results in several problems. First, the focus grid provides a pseudo resolution that can be arbitrarily increased. Similarly to the difference between a spectrum in decibels and a power spectrum density in decibels per hertz, the conventional beamforming result thus is the source power density, e.g. in decibels per cubic meters. Opposed to the pseudo focus grid resolution, conventional beamforming is also limited by the aperture and layout of the array, so that the beamformer output is convoluted with its geometric filter. This results in an expanded main lobe, side lobes, and grating lobes. For multiple sources, large main lobe widths at low

frequencies result in sources, that can no longer be separated, and grating lobes make it difficult to identify the true source position since they are of the same magnitude as the main lobe.

2.3 CLEAN-SC

The first idea to “deconvolve” this geometric filter from the beamformer for astronomy purposes was CLEAN-PSF [17], followed by Clean based on source coherence [23] (CLEAN-SC). It is based on the idea that each focal point represents a compact, incoherent source. Thus, any coherence measured between two focal points originates from the PSF. The coherence between two signals is given by

$$\gamma^2 = \frac{|G_{jk}|^2}{G_{jj}G_{kk}}. \quad (27)$$

CLEAN-SC is based on the idea that the coherence Γ_{jk}^2 between an arbitrary focus point \mathbf{y}_k and all other focus points \mathbf{y}_j can be estimated by steering the CSM to the focus points with

$$\Gamma_{jk}^2 = \frac{|\mathbf{w}_j^\dagger \mathbf{C} \mathbf{w}_k|^2}{(\mathbf{w}_j^\dagger \mathbf{C} \mathbf{w}_j)(\mathbf{w}_k^\dagger \mathbf{C} \mathbf{w}_k)} = \frac{|A_{jk}|^2}{A_{jj}A_{kk}}. \quad (28)$$

Removing the coherent parts of a source removes the PSF (but also distributed sources) from the map. The advantage over CLEAN-PSF, where the theoretical PSF for a monopole source is subtracted from the beamforming map, is that CLEAN-SC “measures” the PSF and thus, is more robust towards the errors in the estimation of the Green’s function (e.g., through complex flows, reflections, and so on). This is performed iteratively with the Algorithm 1, where n is the current iteration, for a maximum number of N iterations, or until a stopping criterion is met. $f \in \mathbf{f}$ is the current frequency, A is the conventional beamforming result for the steering vector \mathbf{w} , and \mathbf{y} is a list of all focus points. \mathbf{C} is the dirty CSM, \mathbf{G} is the CSM of the iteratively identified source, and \mathbf{Q} is the final CLEAN-SC estimation of the “deconvolved” map. For stability, a loop gain $0 < \alpha \leq 1$ is used. The algorithm can be performed with Diagonal Removal (DR) [23] to remove self-noise. Typical stopping criteria for the iterations include a certain dynamic range of the remaining source map compared to the initial maximum or the norm of the remaining CSM.

The method assumes that the global maximum in the beamforming map is the true source position to estimate the source position and strength. While the method is robust towards errors in the localization of the source, one still has to identify the source’s main lobe so that the coherence between the estimated source position and all other focus points yields a meaningful result. Thus, a dense focus grid is necessary to achieve satisfying results, especially at short wavelengths, where the spatial resolution is higher than the focus-grid resolution. However, refining the focus points will only solve this problem partially due to the basis mismatch [7].

If no advanced shading except for DR is used on the CSM, the step of subtracting the clean beam from the dirty CSM can be significantly accelerated. Since the clean beam consists only

Algorithm 1 Standard CLEAN-SC.

FUNCTION CLEAN-SC($\mathbf{C}, \mathbf{w}, \alpha$):

$\mathbf{Q}(\mathbf{f}, \mathbf{y}) \leftarrow \mathbf{0}$

for f **in** \mathbf{f} **do**

$\mathbf{A}_{jj} \leftarrow \mathbf{w}_j^\dagger(f) \mathbf{C}(f) \mathbf{w}_j(f)$

for $n = 1, \dots, N$ **do** ▷ max. number of iterations

$k \leftarrow \text{argmax}_j(\mathbf{A}_{jj})$

$A_{kk} \leftarrow \mathbf{A}_{jj}(\mathbf{y}_k)$ ▷ find pos. of max. amplitude

if $n = 1$ **then**

$A_{kk}^0 \leftarrow A_{kk}$

end if

if $10 \log_{10}(A_{kk}/A_{kk}^0) \leq -\text{SNR}$ **then break**

end if

$\mathbf{h} \leftarrow \frac{\mathbf{C}(f) \mathbf{w}_k(f)}{A_{kk}}$ ▷ find steering vector to the corresp. loc.

if DR **then**

for $n_I = 1, \dots, N_I$ **do** ▷ inner loop iterations

$\mathbf{H} \leftarrow \mathbf{I} \otimes \mathbf{h} \mathbf{h}^\dagger$ ▷ diag. matrix from steering vector

$\mathbf{h} \leftarrow \frac{1}{1 + \mathbf{w}^\dagger \mathbf{H} \mathbf{w}} \left(\frac{\mathbf{C}(f) \mathbf{w}}{\mathbf{w}^\dagger \mathbf{C}(f) \mathbf{w}} + \mathbf{H} \mathbf{w} \right)$ ▷ iteratively find steering vector if DR

end for

end if

$\mathbf{G} \leftarrow A_{kk} \mathbf{h} \mathbf{h}^\dagger$ ▷ clean beam CSM

if DR **then**

$\mathbf{A}_{jj} \leftarrow \mathbf{A}_{jj} - \alpha (|\mathbf{h} \mathbf{w}^\dagger|^2 - \|\mathbf{h} \mathbf{w}^\dagger\|_2^2) A_{kk}$

else

$\mathbf{A}_{jj} \leftarrow \mathbf{A}_{jj} - \alpha (|\mathbf{h} \mathbf{w}^\dagger|^2) A_{kk}$ ▷ subtract clean beam CSM of identified source

end if

$\mathbf{C}^{n-1} \leftarrow \mathbf{C}(f)$ ▷ dirty CSM from the previous loop

$\mathbf{C}(f) \leftarrow \mathbf{C}(f) - \alpha \mathbf{G}$ ▷ subtract identified source from dirty CSM

if $\|\mathbf{C}(f)\|_2 > \|\mathbf{C}^{n-1}\|_2$ **then break** ▷ if the energy in the CSM increases

end if

$\mathbf{Q}(f, \mathbf{y}_k) \leftarrow \mathbf{Q}(f, \mathbf{y}_k) + \alpha A_{kk}$ ▷ add identified source strength to CLEAN-SC output

end for

end for

return $\mathbf{Q}(\mathbf{f}, \mathbf{y})$

of a single component, the beamforming result is simply

$$b = |\mathbf{h} \mathbf{w}^\dagger|^2 A_{kk} \quad (29)$$

and with DR

$$b = (|\mathbf{h} \mathbf{w}^\dagger|^2 - \|\mathbf{h} \mathbf{w}^\dagger\|_2^2) A_{kk} \quad (30)$$

2.4 HR-CLEAN-SC

CLEAN-SC works also, if the estimated source position and true position do not coincide. High-Resolution-CLEAN-SC [24] (HR-CLEAN-SC) utilizes this property to optimize the estimated source positions from an initial CLEAN-SC solution. The originally estimated sources are iteratively moved, so that the influence of each estimated source on each other source is minimized. Algorithm 2 shows the algorithm without DR.

Algorithm 2 HR-CLEAN-SC without DR for a single frequency.

FUNCTION HR-CLEAN-SC($\mathbf{C}, \hat{\mathbf{g}}, \hat{\mathbf{w}}, \alpha, \mu$):
 $\hat{\mathbf{q}} \leftarrow \text{CLEAN-SC}(\mathbf{C}, \hat{\mathbf{w}}, \alpha)$
 $\mathbf{q}, \mathbf{g}, \mathbf{h} \leftarrow \text{nonzero}(\hat{\mathbf{q}})$ ▷ non-zero CLEAN-SC result for unique focus points
 $\mathbf{u} \leftarrow \mathbf{g}$
 $J \leftarrow \text{cardinality}(\mathbf{q})$
for $n = 1, \dots, N$ **do**
 for $j = 1, \dots, J$ **do**
 $\mathbf{u}_j \leftarrow \text{minimize} \left(\frac{\sum_{k=1, k \neq j}^K |\mathbf{g}_k^\dagger \mathbf{u}_j|^2 \|\mathbf{g}_k\|_2^2}{|\mathbf{g}_j^\dagger \mathbf{u}_j|^2 \|\mathbf{g}_j\|_2^2} \right)$ with $|\mathbf{g}_j^\dagger \mathbf{u}_j|^2 \geq \mu > 0$
 end for
 for $j = 1, \dots, J$ **do**
 $\mathbf{h}_j \leftarrow \frac{\mathbf{C}\mathbf{u}_j}{\mathbf{u}_j^\dagger \mathbf{C}\mathbf{u}_j}$
 $\mathbf{A}_{jj}(\hat{\mathbf{w}}_j) \leftarrow \hat{\mathbf{w}}_j^\dagger \mathbf{h} \mathbf{h}^\dagger \mathbf{w}_j$
 $k = \text{argmax}(\mathbf{A}_{jj})$
 $\mathbf{y}_j, \mathbf{w}_j, \mathbf{g}_j \leftarrow \hat{\mathbf{y}}_k, \hat{\mathbf{w}}_k, \hat{\mathbf{g}}_k$
 $\mathbf{q}_j \leftarrow (\mathbf{u}_j^\dagger \mathbf{C}\mathbf{u}_j |\mathbf{w}_j \mathbf{h}_j|^2)$
 end for
end for
return \mathbf{q}, \mathbf{y}

Implementation options for HR-CLEAN-SC for are discussed in the following. The initial CLEAN-SC solution can be obtained with DR or without DR. In our reference implementation, we use a DR solution if HR-CLEAN-SC is also evaluated with DR. Even with a loop gain of $\alpha = 1$ CLEAN-SC can reconstruct sources multiple times on the same focus point. For this paper, we use a unique solution per focus point by adding all sources and steering vectors for the same focus points. In the original publication [24] eq. 28 there may be an error, so that we assume the equation reads

$$\mathbf{h}_1 = \frac{1}{\sqrt{1 + \mathbf{u}_1^\dagger \mathbf{H} \mathbf{u}_1}} \left(\frac{\overline{\mathbf{C} \mathbf{u}_1}}{\mathbf{u}_1^\dagger \mathbf{C} \mathbf{u}_1} + \mathbf{H} \mathbf{u}_1 \right). \quad (31)$$

2.5 B-CLEAN-SC

Broadband-CLEAN-SC (B-CLEAN-SC) [12] aims to relax the problems of CLEAN-SC at high and low frequencies by adapting the idea of broadband Global Optimization [14]: The processing of multiple frequencies at once, so that the side lobes cancel out, but the main lobes add up. This is achieved by introducing a simple change to the CLEAN-SC algorithm: Instead of processing each frequency individually, B-CLEAN-SC processes frequency intervals at once (but still obtains smallband solutions). Here, the only difference lies in determining the location from which the source power is sampled. B-CLEAN-SC averages the dirty maps over the frequency interval and uses the location of the maximum averaged source power. It then performs a standard CLEAN-SC iteration for each of the frequencies in the interval with individual source powers per frequency but at the shared location. Thus, the reconstruction at lower frequencies benefits from the resolution at higher frequencies, and the averaging of side- and grating lobes stabilizes the process at very high frequencies.

B-CLEAN-SC performs each iteration n at a shared location \mathbf{y}_k for all frequencies (within the processed interval \mathbf{f}). To determine the location, instead of using the maximum of the dirty map $\mathbf{A}_{jj}(f)$ separately for each frequency, the maximum of the over frequency averaged dirty map is used

$$k = \operatorname{argmax}_j \left(\left\langle \frac{\mathbf{A}_{ijj}}{\|\mathbf{C}_i\|_2} \right\rangle_i \right), \quad (32)$$

where i denotes the index of the frequency $f_i \in \mathbf{f}$, j denotes the index of the focus point \mathbf{x}_j . The subscript of the average operator $\langle \dots \rangle$ indicates the dimension over which they are applied, in this case the frequency. $\|\mathbf{C}_i\|_2$ is an estimation for the frequency-dependent amplitude of the overall source power (which typically decreases over frequency for aeroacoustic sources). The normalization compensates for this behavior, additionally, DR can be applied. Eq. 32 is the only addition to the CLEAN-SC algorithm to obtain B-CLEAN-SC, see Algorithm 3. The algorithm is given for a frequency interval \mathbf{f} . If the frequency interval does not cover the full frequency range, B-CLEAN-SC is performed sequentially for multiple intervals.

Note that the position \mathbf{y}_k is not necessarily located on the main lobe of a dominant source for all frequencies if the sources have a frequency-dependent power. Especially at low frequencies, where the PSF of a dominant source may cover all other sources and dominate the estimated power at their true positions, this would lead to an overestimation of their power and a subtraction of the main lobe when subtracting coherent portions of the map [24]. A low gain factor α is needed to relax this issue so that the number of necessary B-CLEAN-SC iterations increases. Since only the initial calculation of the dirty map is computationally expensive, the extra iterations are not performance-relevant.

The main relevant implementation detail for this algorithm is when to subtract the clean beam and when to stop the iterations. For the reference implementation, we check (similar to the CLEAN-SC algorithm) if the subtraction of the clean beam results in a norm violation at each frequency. We only perform the subtraction of the clean beam for frequencies where no norm violation occurs. If a norm violation is detected for all frequencies simultaneously, the iterations are stopped.

Algorithm 3 B-CLEAN-SC for a frequency interval \mathbf{f} .

FUNCTION B-CLEAN-SC($\mathbf{C}, \mathbf{w}, \alpha$):

 $\mathbf{Q} \leftarrow \mathbf{0}$
 $\mathbf{A}_{ijj} \leftarrow \mathbf{w}_{ij}^* \mathbf{C}_i \mathbf{w}_{ij}$
for $n = 1, \dots, N$ **do**
 $\hat{\mathbf{A}}_{jj} \leftarrow \left\langle \frac{\mathbf{A}_{ijj}}{\max_j(\mathbf{A}_{ijj}^0)} \right\rangle_i$
 $k \leftarrow \operatorname{argmax}_j(\hat{\mathbf{A}}_{jj})$
 \triangleright change to the CLEAN-SC algorithm

 $\mathbf{A}_{ikk} \leftarrow \mathbf{A}_{ijj}(\mathbf{y}_k)$
 $\mathbf{h}_f \leftarrow \frac{\mathbf{C}_i \mathbf{w}_{ik}}{\mathbf{A}_{ikk}}$
if DR **then**
 $\mathbf{H}_{ikk} \leftarrow \mathbf{h}_{ik} \mathbf{h}_{ik}^* \mathbf{I}_{kk}$
 $\mathbf{h}_{ik} \leftarrow \frac{1}{1 + \mathbf{w}_{ik}^* \mathbf{H}_{ikk} \mathbf{w}_{ik}} \left(\frac{\mathbf{C}_i \mathbf{w}_{ik}}{\mathbf{w}_{ik}^* \mathbf{C}_i \mathbf{w}_{ik}} + \mathbf{H}_{ikk} \mathbf{w}_{ik} \right)$
end if
 $\mathbf{C}^{n-1} \leftarrow \mathbf{C}(f)$
 $\hat{i} \leftarrow \operatorname{argwhere}(\|\mathbf{C}\|_2 < \|\mathbf{C}^{n-1}\|_2)$
if $i = \hat{i}$ **then break**
end if
 $\mathbf{G}_{\hat{i}} \leftarrow \mathbf{A}_{\hat{i}kk} \mathbf{h}_{\hat{i}} \mathbf{h}_{\hat{i}}^\dagger$
 $\mathbf{C}_{\hat{i}} \leftarrow \mathbf{C}_{\hat{i}} - \alpha \mathbf{G}_{\hat{i}}$
 $\hat{\mathbf{A}}_{ijj} \leftarrow \mathbf{A}_{ijj} - \alpha \mathbf{w}_{ij}^* \mathbf{G}_{\hat{i}} \mathbf{w}_{ij}$
 $\mathbf{Q}(f_i, \mathbf{y}_k) \leftarrow \mathbf{Q}(f_i, \mathbf{y}_k) + \alpha \mathbf{A}_{ikk}$
end for
return $\mathbf{Q}(\mathbf{f}, \mathbf{y})$

2.6 Local Optimization

Local Optimization is a CSM fitting method (CFM). Based on a source assumption, such as the source position, the source strength, and the source type, the Green's matrix is constructed, and a synthetic CSM is calculated. The synthetic CSM is then compared to the measured CSM via any norm (typically the l_1 or l_2 -norm), also called the cost function, or energy function E . The norm can be applied to the upper triangular matrix, which is effectively equal to DR, as it ignores self-noise. The assumed variables such as the source position and strength are then optimized, to minimize the norm. The advantage is that CMF methods do not impose any limitations on the model, such as compact monopoles, fixed focus points, or incoherent sources, and do not need a normalized steering vector so that they can identify both the correct source location and level.

Von den Hoff et al. [26] suggests the MSE between the measured CSM \mathbf{c}_{meas} and the synthetic CSM \mathbf{c}_{syn} for the upper triangular matrix \tilde{i} , that is

$$E(f) = \sum_{\tilde{i}} (|\mathbf{c}_{\text{syn}, \tilde{i}}(f) - \mathbf{c}_{\text{meas}, \tilde{i}}(f)|^2) \quad . \quad (33)$$

to solve eq. 5, and effectively find \mathbf{q} and \mathbf{T} . The problem for CFM methods is that the norm is typically nonlinear and non-convex. Thus, global optimization [19] can be employed, which is extremely time-consuming, and not guaranteed to find the global optimum [6, 14, 21].

Given, that the initial guess for the source positions is good enough, the global search problem reduces to a local search problem [14], also called Local Optimization (LO). Especially for the amplitude the cost function is convex, given that the source position is correct. This paper uses this observation to propose a hybrid approach: First, source positions are identified with B-CLEAN-SC (preferably with steering vector formulation IV to find the correct locations). Second, the identified source positions and amplitudes are then used as initial guesses for LO. For the sake of speed and robustness, only the amplitudes are further optimized, but again, LO could also be used to find dipole rotations, optimize the speed of sound, or other parameters [14].

2.7 Regions Of Interest

A challenge for all beamforming methods that calculate results independently for each frequency is that generating a spectrum is not trivial. The first challenge is, that it is typically unknown how many sources are located within the map, how they are distributed, and in which frequency ranges they can be observed. The second challenge is, that true sources are masked by artifacts such as side-lobes of other sources. The third challenge is how to extract the optimal spectra from the beamforming map.

Conventional beamforming produces dense maps so that each focus point contains a source strength $q(y, f) > 0 \text{ Pa}^2 \text{ Hz}^{-1}$. Here, the source identification and spectra generation problem is particularly difficult. Even when summing all frequencies to obtain an Overall Sound Pressure Level (OASPL), the map is still multi-dimensional and difficult to visualize and analyze.

CLEAN-SC [23] and its derivatives produce sparse maps, which means that only a few focus points contain a source strength $q(y, f) > 0 \text{ Pa}^2 \text{ Hz}^{-1}$. Here, one can use this sparseness property to identify source positions based on the statistical spatial occurrence of source-parts directly using clustering [15, 18].

For simple problems with few sources, many results rely on manually defined Regions Of Interest (ROI). These are spatial regions that define a source and assign each location within them to the source. When two ROI spatially overlap, a focus point is assigned to the source with the closest distance to the ROI midpoint. Focus points that are not located in any ROI are rejected as background noise. For the simple problems in this paper, the ROIs are defined manually for repeatability based on the ground truth, and based on the extensive analysis of the Dornier data [13, 16].

3 Data

This section presents the data used for this paper. The ground truth sources are labeled with Roman numbers, estimated sources (e.g., via ROI) are labeled with Arabic numbers.

3.1 Case 1) - 1D synthetic monopole

Case 1) features synthetic data in the frequency domain without noise. The frequencies are $32\text{Hz} \leq f \leq 8192\text{Hz}$ with $\Delta f = 32\text{Hz}$. Three sources are located at

$$\begin{bmatrix} y_I \\ y_{II} \\ y_{III} \end{bmatrix} = \begin{bmatrix} 0.0 & 0.5 & 0.0 \\ 0.1 & 0.5 & 0.0 \\ 0.5 & 0.5 & 0.0 \end{bmatrix} \quad (34)$$

The array consists of 21 sensors at $y = z = 0\text{m}$, $-0.5\text{m} \leq x \leq 0.5\text{m}$ with $\Delta x = 0.05\text{m}$. There are 501 focus points at $y = 0.5\text{m}, z = 0\text{m}$, $1\text{m} \leq x \leq 1\text{m}$ with $\Delta x = 0.004\text{m}$. Figure 1 shows the setup, the focus points which are assigned to the different sources are displayed in color.

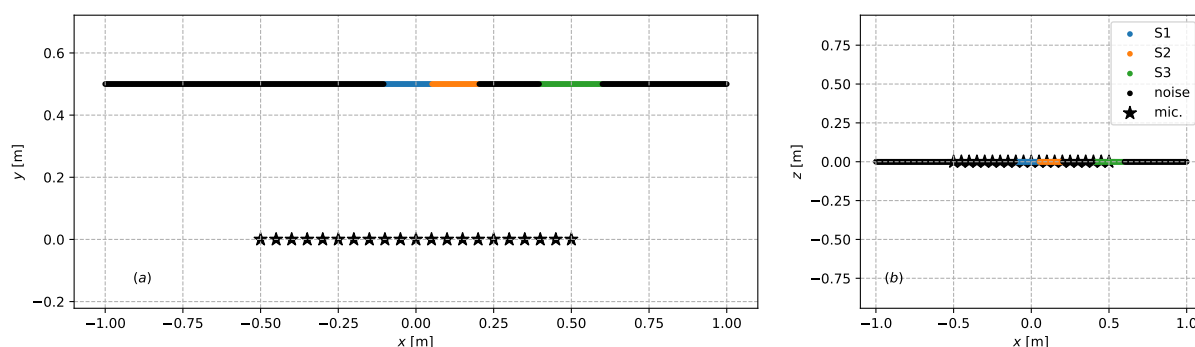


Figure 1: Case 1a), setup of the synthetic data, showing the equidistant 1D line array (*), the focus points at $\Delta y = 0.5\text{m}$, and the ROIs, covering the three true source locations.

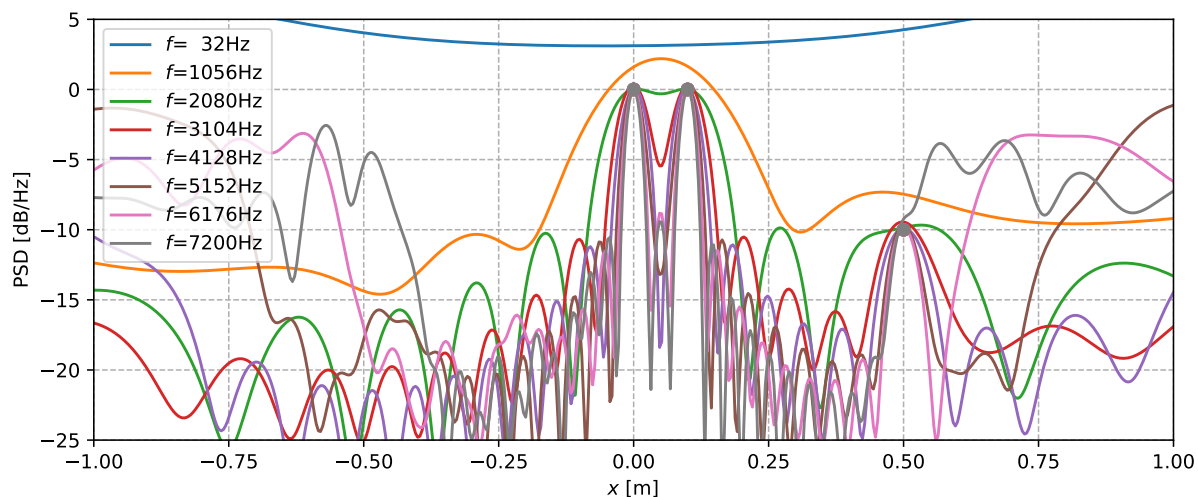


Figure 2: Case 1a), PSD estimation via conventional beamforming for three sources at $L_I=0\text{dB Hz}^{-1}$, $L_{II}=0\text{dB Hz}^{-1}$, $L_{III}=-10\text{dB Hz}^{-1}$.

The case features two sub-cases: For case 1a) the amplitudes of the sources are constant over frequency with $L_I=0 \text{ dB Hz}^{-1}$, $L_{II}=0 \text{ dB Hz}^{-1}$, $L_{III}=-10 \text{ dB Hz}^{-1}$, as shown in Figure 2. For case 2b) the amplitude L_I increases linearly over frequency from $L_I=-10 \text{ dB Hz}^{-1}$ to $L_I=0 \text{ dB Hz}^{-1}$, while the amplitude of source II decreases in the same way. Source III is a smallband source at $3584 \text{ Hz} \leq f \leq 3840 \text{ Hz}$ with $L_{III} = -10 \text{ dB Hz}^{-1}$. Figure 2 shows the array performance for case 1a). Strong sidelobes are visible throughout the frequency range due to the equidistant sensor spacing. Below $f \leq 2 \text{ kHz}$ the two sources in the center can no longer be resolved individually.

3.2 Case 2) - 2D synthetic monopole

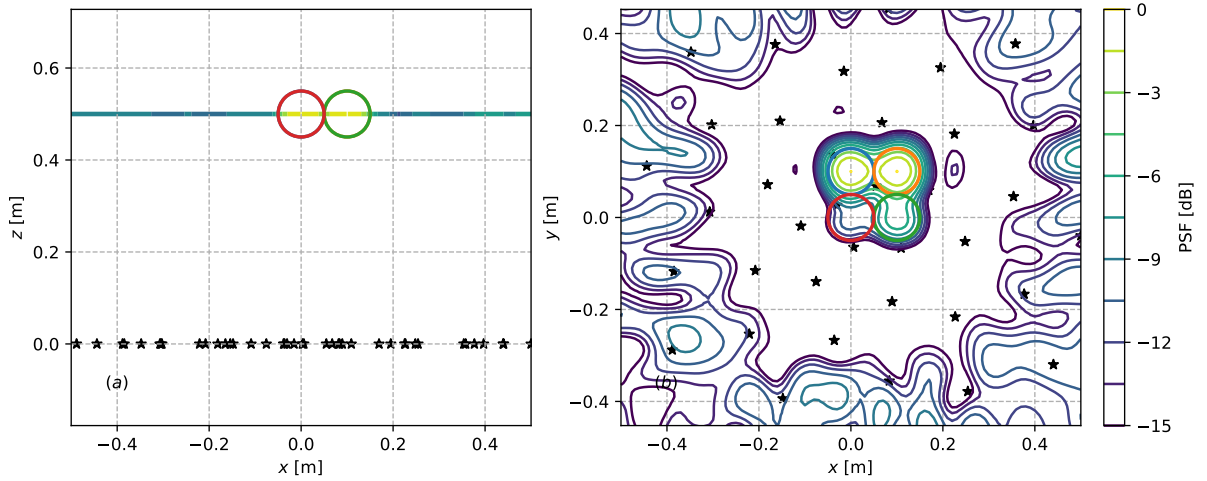


Figure 3: Case 2), PSD estimation at $f = 3008 \text{ Hz}$ via conventional beamforming for four sources at $L_I=0 \text{ dB Hz}^{-1}$ (blue), $L_{II}=0 \text{ dB Hz}^{-1}$ (orange), $L_{III}=-5 \text{ dB Hz}^{-1}$ (green), $L_{IV}=-10 \text{ dB Hz}^{-1}$ (red).

Case 2) features synthetic data in the frequency domain without noise. The frequencies are $32 \text{ Hz} \leq f \leq 8192 \text{ Hz}$ with $\Delta f = 32 \text{ Hz}$. Three sources are located at

$$\begin{bmatrix} y_I \\ y_{II} \\ y_{III} \\ y_{IV} \end{bmatrix} = \begin{bmatrix} 0.0 & 0.1 & 0.5 \\ 0.1 & 0.1 & 0.5 \\ 0.1 & 0.0 & 0.5 \\ 0.0 & 0.0 & 0.5 \end{bmatrix} \quad (35)$$

The array consists of 41 sensors at $z = 0 \text{ m}$, $1 \text{ m} \times 1 \text{ m}$ aperture with Fermat spacing (rectangular cutout). There are 101×101 focus points at $z = 0.5 \text{ m}$, $-0.5 \text{ m} \leq x, y \leq 0.5 \text{ m}$. Figure 3 shows the setup and the 2D conventional beamforming result with steering vector III at $f \approx 3 \text{ kHz}$, and four circular ROI with a diameter $d = 0.1 \text{ m}$ around the true source locations are displayed.

3.3 Case 3) - Generic 2D monopole

The data features an equidistant 7x7 microphone array $-0.27\text{ m} \leq x, y \leq 0.27\text{ m}$, $z = -0.65\text{ m}$, with $\Delta x = \Delta y = 0.09\text{ m}$. The source is a generic monopole source (streamlined housing with a circular $d = 5\text{ mm}$ opening at the downstream end). It is moved to the three locations

$$\begin{bmatrix} y_I \\ y_{II} \\ y_{III} \end{bmatrix} = \begin{bmatrix} -0.05 & 0.1 & 0.0 \\ 0.10 & 0.1 & 0.0 \\ 0.25 & 0.1 & 0.0 \end{bmatrix} \quad (36)$$

during separate measurements and uses uncorrelated white noise with different band-pass frequencies and amplitudes to generate different spectra. The ground truth source powers are obtained by dividing the individual CSMs by the Green's matrices of an ideal monopole. Then, the absolute upper triangular CSM entries \bar{i} are averaged to obtain an average ground truth spectrum with standard deviation. Thus, the ground truth excludes self-noise since it does not use the CSM diagonal.

$$\text{PSD}_{\text{true}}(f) = \left\langle \left| \frac{\mathbf{C}(f)}{\mathbf{G}(f)} \right| \right\rangle_{\bar{i}} \quad (37)$$

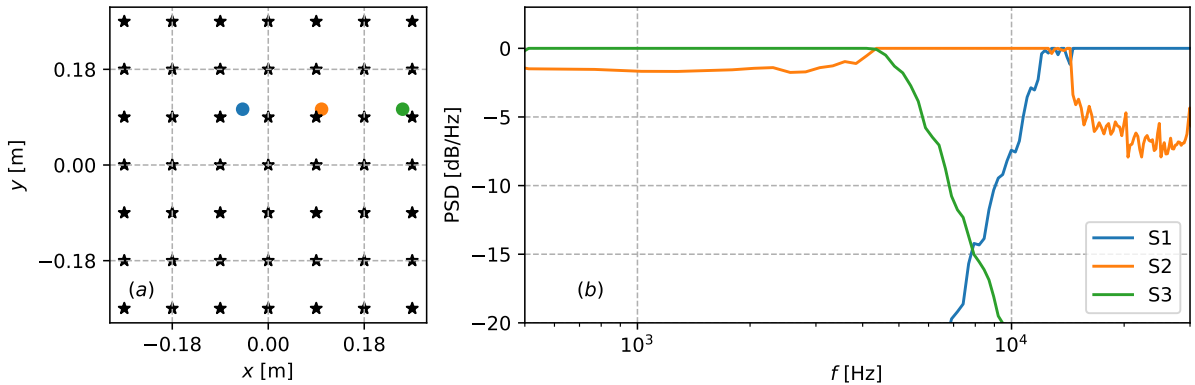


Figure 4: Case 3), ground truth. (a) shows the spatial position of the three sources, (b) shows the normalized, average spectra and their standard deviation based on eq. 37.

The ground truth is normalized, so that the maximum of the three sources at each frequency is $L_{\text{max}} = 0\text{ dB Hz}^{-1}$. The corresponding CSMs are normalized in the same way. Figure 4 shows the resulting setup, and ground truth spectra. Up to $f \leq 4\text{ kHz}$ S_{III} is dominant, and S_{II} is about $\Delta L \approx 1.5\text{ dB}$ quieter. Above this frequency, S_{III} is attenuated with -15 dB per octave, and S_{II} is dominant. At $f \geq 12\text{ kHz}$ S_I is dominant.

To evaluate how close the real sound source is to an ideal monopole, a synthetic CSM is generated based on the average ground truth spectra, see eq. 37, the true source locations, and the compact monopole assumption. Thereafter, the Mean Absolute Error (MAE) of the upper triangular synthetic and measured CSM is calculated to measure the distance of the assumption and data. The complex CSMs are subtracted, and then the absolute and angle are analyzed.

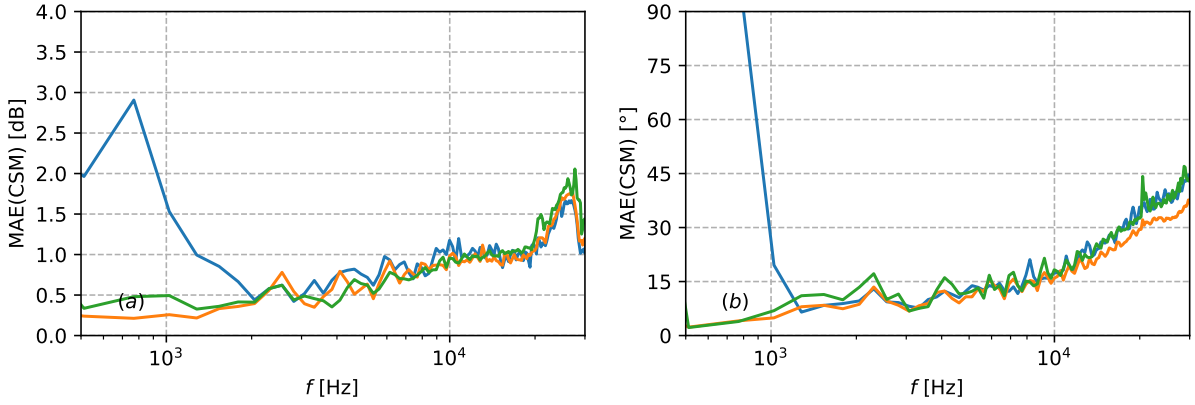


Figure 5: Case 3), MAE between synthetic CSM based on assumed ground truth and real data for (a) the absolute MAE and (b) the angle.

Figure 5 shows the resulting MAE, which is calculated for the absolute PSD difference (a) and absolute phase difference (b). The errors show that the monopole assumption is reasonable at low frequencies and is gradually violated at increasing frequencies by the speaker design (non-compactness, asymmetric orientation towards the array). Note, that at low frequencies the large error of S_I is neglectable, due to the low Signal-to-Signal-Ratio (SSR). It will be of particular interest how different methods perform at these very low and high frequencies, where the compact monopole assumptions are violated.

The three normalized CSMs are super-positioned (addition) to obtain a single CSM that contains three incoherent sources.

3.4 Case 4) - Dornier 728 closed wind tunnel 2D

To test the algorithms on challenging real data, this paper uses the dataset of a Dornier 728 in a closed test section [1] at $Re \approx 1.4 \times 10^6$ for a mean aerodynamic cord length of $D_0 = 0.353$ m. The angle of attack is $\alpha = 1^\circ$, and the Mach number is $M = 0.125$. Due to the low Mach number, the data features relatively low background noise levels, but due to the low angle of attack, the model is also very quiet.

The array consists of 144 microphones at an oval aperture of $1.756 \text{ m} \times 1.3 \text{ m}$, and the data is sampled at $f_S = 120 \text{ kHz}$. The CSM is calculated using Welch's method with a block size of 2^8 samples and 50% overlap, resulting in 128 frequencies. An equidistant 2D focus grid with a resolution of $\Delta x = 0.01 \text{ m}$ spans the entire wing $-0.3 \text{ m} \leq x \leq 0.8 \text{ m}$, $-0.7 \text{ m} \leq z \leq 0.7 \text{ m}$. The focus plane is around $\Delta y \approx 1 \text{ m}$ away from the array.

4 Results

This section shows the results of the discussed methods for the different cases.

Table 1: Relative computation times to case 1) CLEAN-SC ($t = 2.1$ s with standard Intel i5 laptop) of the different methods and cases, number of focus points (fcp) and microphones (mic).

Case	1a)	1b)	2)	3)	4)
fcp.	501	501	10201	14641	15651
mic.	21	21	41	49	144
CLEAN-SC	1x	0.8x	47x	110x	142x
HR-CLEAN-SC	113x	67x	303x	1976x	-
B-CLEAN-SC	9x	10x	126x	97x	1704x

4.1 Case 1)

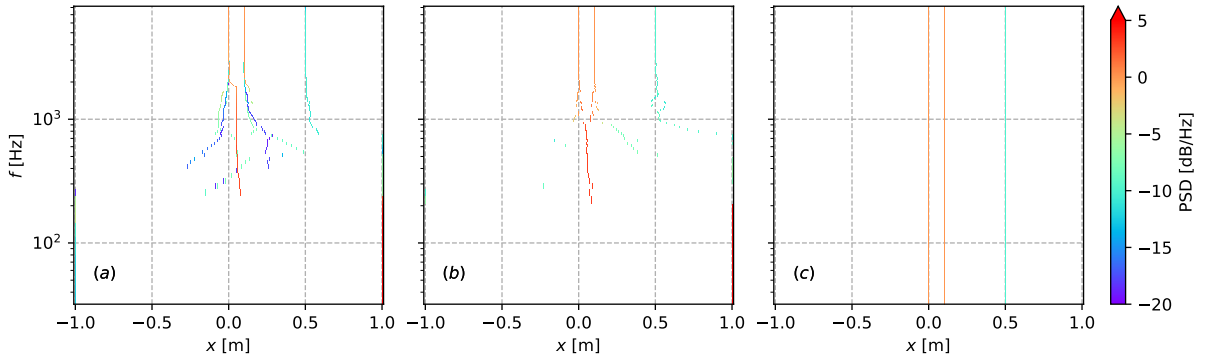


Figure 6: Case 1a), sparse source reconstruction on the 1D focus grid for (a) CLEAN-SC, (b) HR-CLEAN-SC, (c) B-CLEAN-SC with LO, all without DR.

For case 1) CLEAN-SC is run with steering vector III, $\alpha = 0.9$, a maximum of $N = 10$ iterations, and a maximum SNR of 20dB without DR. HR-CLEAN-SC is run with $\alpha = 1, \mu = 0.25$, SNR = 15dB, $N = 10$, steering vector III. B-CLEAN-SC is run with $\alpha = 1, N = 10$, SNR = 30dB, steering vector IV, at all frequencies simultaneously, and LO is applied afterwards to optimize the source amplitudes (but not the source positions).

Figure 6 shows the different methods' results for case 1a). Figure 6 (a) shows that below $f \leq 2$ kHz CLEAN-SC estimates a single, dominant source in the middle of S_I and S_{II} , due to the low array resolution. There are two additional weak sources that move with decreasing frequency away from the correct location. Figure 6 (b) shows that below $f \leq 200$ Hz CLEAN-SC cannot resolve a main-lobe, so that all energy is reconstructed at the outer edge of the focus grid. HR-CLEAN-SC estimates the source positions correctly down to $f = 1$ kHz, and thus halving the resolvable frequency. Below, similar effects as in the CLEAN-SC solution appear. Figure 6 (c) shows that B-CLEAN-SC estimates the source positions correctly, which is by definition shared for all frequencies, as well as the source amplitudes.

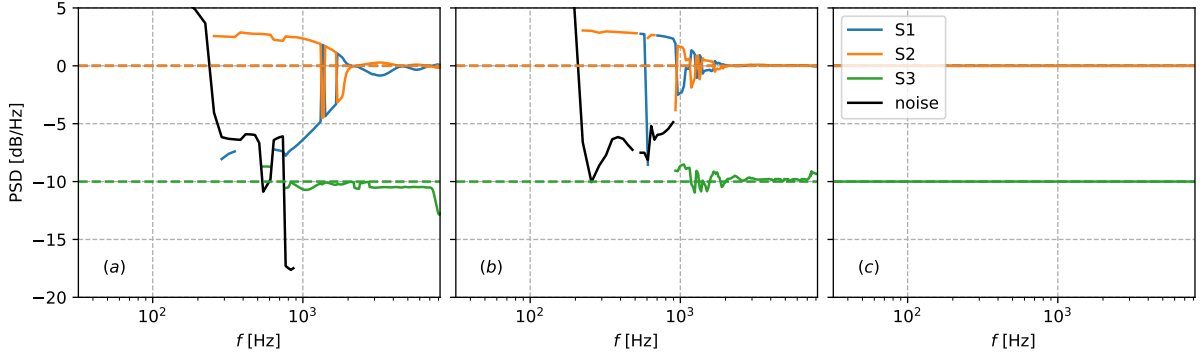


Figure 7: Case 1a), spectra from the spatially integrated maps for the ROIs in Figure 1. The ground truth is depicted with dashed lines, the ROI estimation with full lines. (a) shows CLEAN-SC, (b) shows HR-CLEAN-SC, and (c) shows B-CLEAN-SC results with LO, all without DR.

Figure 8 shows the corresponding source spectra estimations, based on the ROIs in Figure 1. The dominant estimation by CLEAN-SC between S_I and S_{II} periodically iterates between S_1 and S_2 , resulting in unsteady spectral estimations. This is a severe issue when the scaling of sources is evaluated (e.g., Strouhal versus Helmholtz number at different Mach numbers), since this effect is always coupled to the Helmholtz number [16]. Above $f \geq 2$ kHz CLEAN-SC estimates the source levels correctly with small errors. Between $1 \text{ kHz} \leq f \leq 2 \text{ kHz}$ the periodical oscillations between S_1 and S_2 make the spectral estimation unreliable. Between $300 \text{ Hz} \leq f \leq 1 \text{ kHz}$ the dominant source region (not the individual sources) is resolved somewhat correctly, assuming that the addition of two incoherent sources results in $\Delta \text{PSD} = 3 \text{ dB}$. Below $f \leq 300 \text{ Hz}$ there is no meaningful result. The weak source is estimated correctly down to $f \geq 800 \text{ Hz}$. HR-CLEAN-SC estimates the spectra similarly, but the periodical oscillations between S_1 and S_2 are fully suppressed from $f \geq 2 \text{ kHz}$, and much weaker for $1 \text{ kHz} \leq f \leq 2 \text{ kHz}$, so that the estimation is much more reliable. The total source region is estimated down to $f \geq 200 \text{ Hz}$. For the weak source there is no difference between HR-CLEAN-SC and CLEAN-SC. B-CLEAN-SC with LO for the spectral estimation estimates all sources perfectly throughout the frequency range. There is also no noise (estimations outside of any ROI).

Figure 8 shows the source spectra estimations for case 1b) with frequency-dependent source amplitudes. CLEAN-SC and HR-CLEAN-SC estimate the sources similarly. The dominant source S_{II} is estimated correctly down to $f \geq 200 \text{ Hz}$. The weaker source S_I is estimated from $f \geq 800 \text{ Hz}$. While CLEAN-SC underestimates its level with decreasing frequency, HR-CLEAN-SC correctly predicts its level down to low frequencies. Both methods identify the small-band source perfectly. B-CLEAN-SC with LO estimates all sources throughout the frequency range perfectly without noise.

4.2 Case 2)

For case 2) CLEAN-SC is run with steering vector III, $\alpha = 0.9$, $N = 20$, and a maximum SNR of SNR = 20 dB without DR. HR-CLEAN-SC is run with $\alpha = 1$, $\mu = 0.25$, SNR = 15 dB, $N = 20$, steering vector III without DR. B-CLEAN-SC is run with $\alpha = 1$, $N = 10$, SNR = 30 dB,

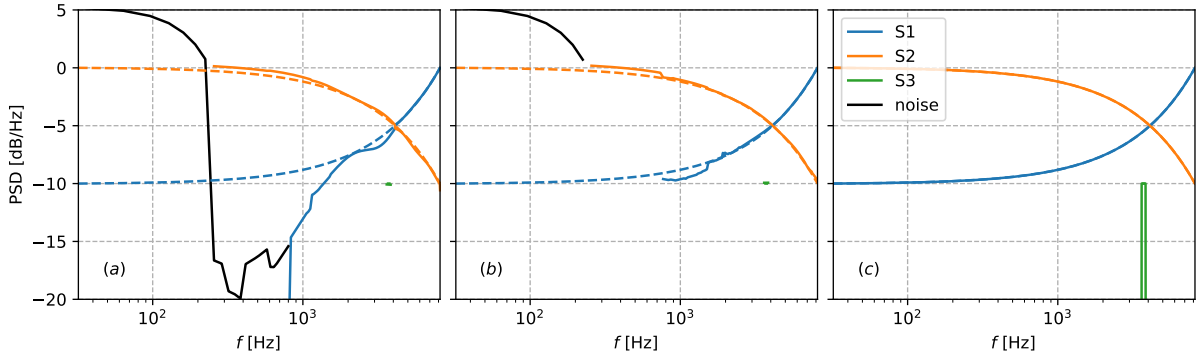


Figure 8: Case 1b), spectra from the spatially integrated maps for the ROIs in Figure 1. The ground truth is depicted with dashed lines, the ROI estimation with full lines. (a) shows CLEAN-SC, (b) shows HR-CLEAN-SC, and (c) shows B-CLEAN-SC results with LO, all without DR.

steering vector IV, at all frequencies simultaneously, and LO, without DR.

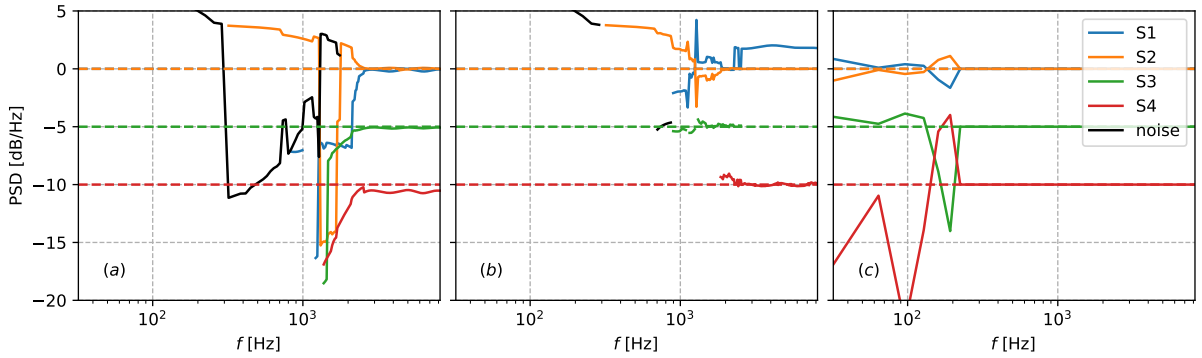


Figure 9: Case 2), spectra from the spatially integrated maps for the ROIs in Figure 3. The ground truth is depicted with dashed lines, the ROI estimation with full lines. (a) shows CLEAN-SC, (b) shows HR-CLEAN-SC, and (c) shows B-CLEAN-SC results with LO, all without DR.

Due to the same aperture and spacing of the sources, the results are similar to the 1D case 1). Figure 9 shows the CLEAN-SC correctly estimates source levels for $f \geq 2$ kHz, between $1 \text{ kHz} \leq f \leq 2 \text{ kHz}$ the periodical oscillations appear, between $300 \text{ Hz} \leq f \leq 1 \text{ kHz}$ the dominant source region is resolved correctly, and below no meaningful result is obtained. HR-CLEAN-SC shows fewer oscillations, but for some reason, the levels of S_I are over-predicted at high frequencies. B-CLEAN-SC and LO estimate the source levels correctly down to $f \geq 200$ Hz, below which oscillations and errors occur. While the dominant two sources are somewhat correctly estimated throughout the whole frequency range some of the energy leaks between the sources, the that their total power is correct, but not their individual power. Between the weak sources S_{III} and S_{IV} there is a confusion of sound powers at $f = 200$ Hz, and below S_{IV} is

insufficiently reconstructed. Note, that the method does not produce noise.

4.3 Case 3)

For case 3) with real data CLEAN-SC is run with steering vector III, $\alpha = 0.9$, $N = 20$, and a maximum SNR of $\text{SNR} = 40\text{dB}$ without DR. HR-CLEAN-SC is run with $\alpha = 1$, $\mu = 0.25$, $\text{SNR} = 40\text{dB}$, $N = 20$, steering vector III without DR. B-CLEAN-SC is run with $\alpha = 1$, $N = 20$, $\text{SNR} = 30\text{dB}$, steering vector IV, at all frequencies simultaneously, and LO, without DR.

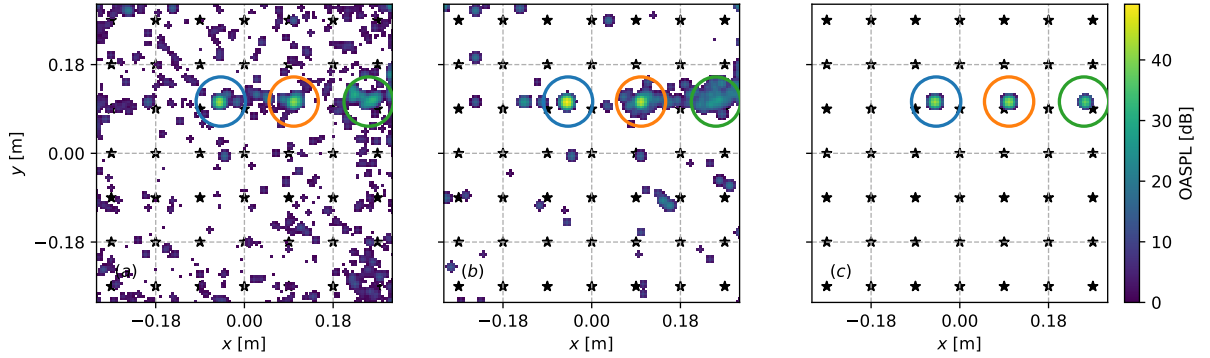


Figure 10: Case 3), $OASPL(x,y)$ for (a) CLEAN-SC, (b) HR-CLEAN-SC, and (c) B-CLEAN-SC with LO, all without DR. A Gaussian convolution is applied to the results for better visibility of the sparse source distribution with $\sigma = 0.005\text{ m}$.

Figure 10 shows the Overall Sound Pressure Level (OASPL), which is the source map integrated over all frequencies. The results are fairly similar for all methods. CLEAN-SC produces lots of noise, but the main sources are clearly visible. S_{III} appears slightly smeared out. HR-CLEAN-SC results in less noise, but S_{III} is smeared out completely. B-CLEAN-SC estimates the source positions correctly without noise.

Figure 11 shows the integrated spectra. CLEAN-SC estimates S_I correctly for $f \geq 6\text{ kHz}$, below which some artifacts appear. S_{II} is estimated correctly from $f \geq 2\text{ kHz}$, apart from $f \approx 20\text{ kHz}$. S_{III} is estimated correctly for $f \geq 700\text{ Hz}$, up to $f \leq 10\text{ kHz}$, above which artifacts appear. The noise level is about -15 dB to -10 dB , and sources are estimated down to a $SSR \geq -20\text{ dB}$. HR-CLEAN-SC shows worse source-level estimations. The spectra oscillate strongly over frequency and the overall source levels are off. Sources are somewhat reconstructed down to $SSR \geq -10\text{ dB}$. B-CLEAN-SC with LO estimates the source levels similar to CLEAN-SC with some major differences. S_I is also estimated correctly for $f \geq 6\text{ kHz}$, however, below there are strong oscillations, and below $f \leq 2\text{ kHz}$ the source is estimated consistently as a dominant source. S_{II} is estimated correctly from $f \geq 600\text{ Hz}$ throughout the full frequency range. S_{III} is estimated correctly up to $f \leq 10\text{ kHz}$, above which strong oscillations appear. There is no noise, and sources are estimated down to a $SSR \geq -20\text{ dB}$.

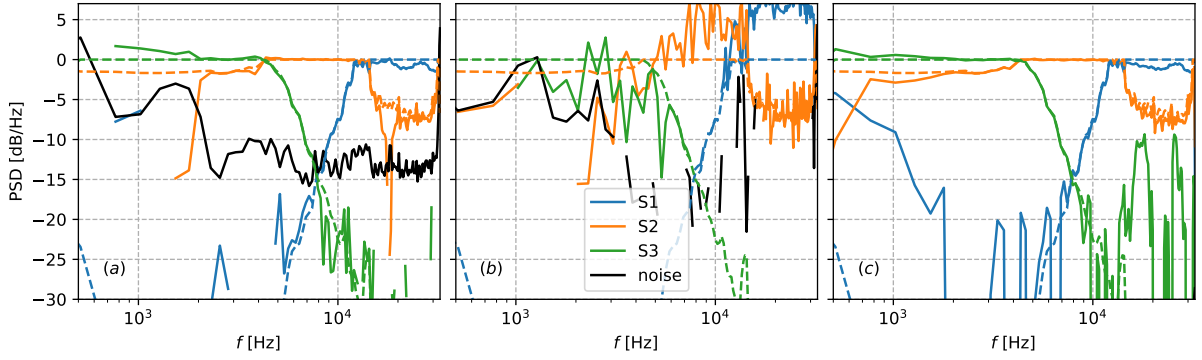


Figure 11: Case 3), spectra from the spatially integrated maps for the ROIs in Figure 3. The ground truth is depicted with dashed lines, the ROI estimation with full lines. (a) shows CLEAN-SC, (b) shows HR-CLEAN-SC, and (c) shows B-CLEAN-SC results with LO, all without DR.

4.4 Case 4)

For case 3) with real data CLEAN-SC is run with steering vector III, $\alpha = 0.9$, $N = 50$, and a maximum SNR of $\text{SNR} = 30\text{dB}$ with DR. Due to issues with the HR-CLEAN-SC implementation with DR, the method's results are neglected here. B-CLEAN-SC is run with $\alpha = 0.9$, $N = 50$, $\text{SNR} = 30\text{dB}$, steering vector III, for frequency intervals of 32 frequencies at once, without LO, with DR.

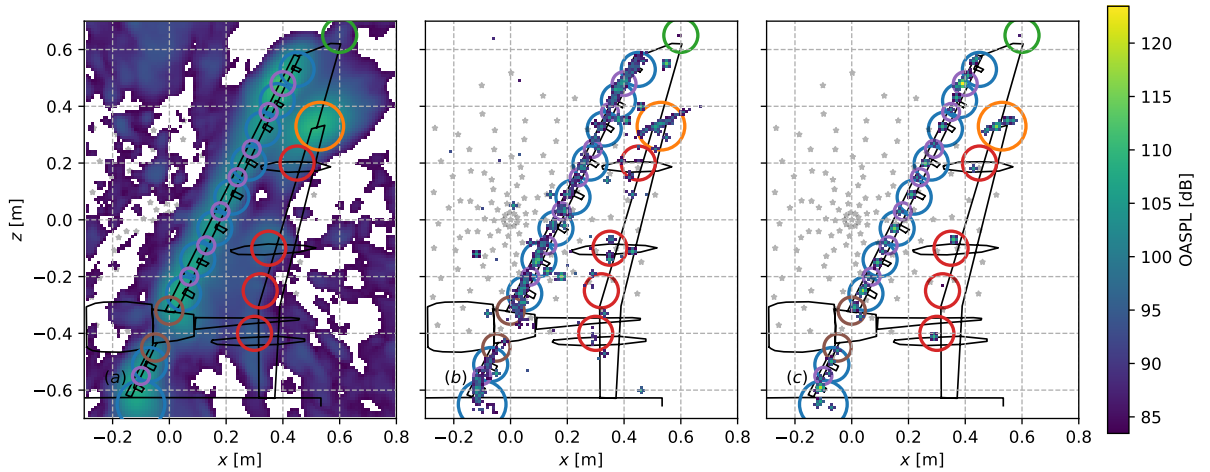


Figure 12: Case 4), $\text{OASPL}(x, z)$ for (a) conventional beamforming, (b) CLEAN-SC, and (c) B-CLEAN-SC without LO, all with DR. Circular ROI are marked with different colors.

Figure 12 shows OASPL for (a) conventional beamforming, (b) CLEAN-SC, and (c) B-CLEAN-SC. The conventional map resolves the main source regions, which are the slat, the flap, and the wing tip. Different ROI are defined based on an extensive source analysis [13].

CLEAN-SC reconstructs the main source regions well with some noise. B-CLEAN-SC reconstructs the source regions similarly, without noise.

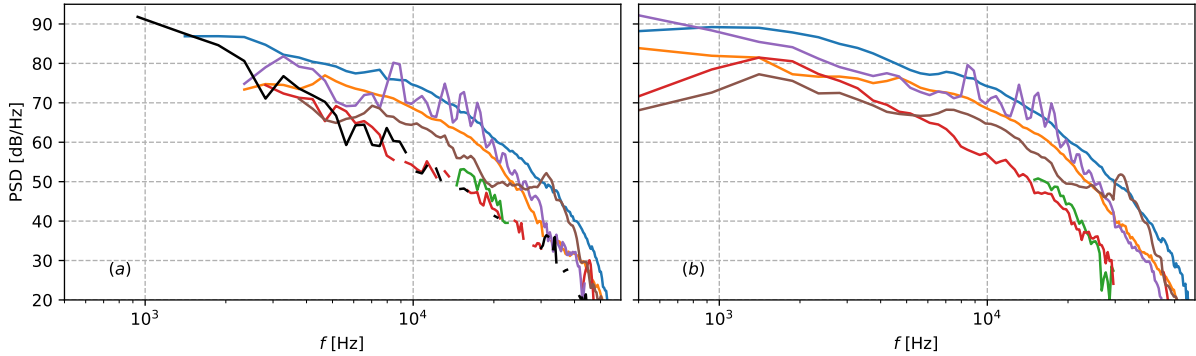


Figure 13: Case 4), spectra from the spatially integrated maps for the ROIs in Figure 12, black lines indicate noise. No ground truth is available. (a) shows CLEAN-SC, (b) shows B-CLEAN-SC results.

Figure 13 shows the resulting spectra. In the valid frequency range of CLEAN-SC both methods produce very similar spectra. However, B-CLEAN-SC is able to obtain a wider range of valid spectra for the flap region (red) and the wing tip (green). Further, the CLEAN-SC result is contaminated with noise at a level similar of the weaker sources.

5 Discussion

The results of case 1) and case 2) showed that HR-CLEAN-SC yields an advantage over CLEAN-SC, effectively halving the resolvable frequency, which corresponds to the observation of the original work [24]. However, for the real data in case 3) HR-CLEAN-SC struggled, whereas CLEAN-SC produced stable results within its known limitations at low frequencies. Unfortunately, no HR-CLEAN-SC results were obtained for case 4), since the reference implementation with DR is not stable. B-CLEAN-SC performs extremely well on synthetic data without noise. The combination of steering vector IV allows for the determination of the correct source positions, which in return allows for the LO of the source powers. Due to the reasonable initial values, the optimizer converges fast and yields the correct source powers. For real data, the method is limited by the dynamic range of the setup, which depends on both the number of microphones and Welch block averages. For the generic open wind tunnel case, thus, B-CLEAN-SC was not able to reconstruct source levels at an SSR below the CLEAN-SC solution. Additionally, the monopole violation and very low SSR result in an overestimation of source power by LO, already observed for global optimization [14]. For the closed wind tunnel experiment the combination of B-CLEAN-SC with LO failed so that B-CLEAN-SC without LO and steering vector III was performed. The reason for this is that the CSM is dominated by shear layer noise, which is partially coherent, especially at low frequencies. Thus, LO tries to minimize the shear layer noise, instead of the aeroacoustic noise, which fails. B-CLEAN-SC performs well without LO but is then limited by the initial issue that we cannot obtain both the correct source location and source power. However, in real-world scenarios, it

is often sufficient to locate the source position to a certain degree. Additionally, the broadband approach of B-CLEAN-SC enhances the location estimation. The result is a noise-free source map with well-resolved spectra down to low frequencies, whereas CLEAN-SC results in lots of noise and is strongly limited by the array's aperture and geometry. Apparently, B-CLEAN-SC can also resolve distributed sources, such as the flap side edge in Figure, which, however, results in more iterations, which have to be performed for multiple frequencies, even if the source is a small-band source.

Performance wise CLEAN-SC is very fast. Since it relies only on matrix multiplications, it can be accelerated and parallelized to a high degree. HR-CLEAN-SC on the other is computationally expensive, due to the inherent optimization process. Since B-CLEAN-SC is basically CLEAN-SC at a shared focus point, the B-CLEAN-SC iterations are as fast as CLEAN-SC. If LO is used, it adds extra computational time. If it is not, a lower gain factor may result in additional B-CLEAN-SC loops. In total, B-CLEAN-SC is about 10x slower than CLEAN-SC in the current Python reference implementation.

6 Conclusion

CLEAN-SC is up to this day the gold standard in closed wind tunnel testing because it is fast and robust. Its limitations are mainly distributed and coherent sources, as well as high noise levels throughout the frequency range, and the source estimation at low and high frequencies because of the Rayleigh limit and grating lobes. While HR-CLEAN-SC is able to effectively halve the frequency at which sources can be reconstructed, the reference implementation of the method is slow and produces unwanted artifacts at high frequencies. B-CLEAN-SC introduces a simple addition to CLEAN-SC so that frequency intervals are processed in parallel at a shared location, which stabilizes the process and allows for the reconstruction of sources at low and high frequencies while suppressing noise. The addition of local optimization allows for further improved spectral estimations, but only for scenarios with low correlated background noise levels, such as open wind tunnels, but not closed wind tunnels, where the partially coherent shear layer dominates the CSM. Thus, B-CLEAN-SC without local optimization is a suited candidate to replace CLEAN-SC in closed wind tunnel experiments to extend the observable frequency towards lower frequencies, but it is not suited to further enhance the knowledge of coherent and distributed sources.

Acknowledgment

I would like to thank Pieter Sijtsma and Gilles Chardon for the fruitful discussions about HR-CLEAN-SC and help with the reference implementation. Further, I would like to thank Daniel Ernst for the discussions about CLEAN-SC and steering vectors.

References

- [1] T. Ahlefeldt. "Aeroacoustic measurements of a scaled half-model at high reynolds numbers." *AIAA J.*, 51(12), 2783–2791, 2013. doi:10.2514/1.J052345.

- [2] T. Ahlefeldt, D. Ernst, A. Goudarzi, H.-G. Raumer, and C. Spehr. “Aeroacoustic testing on a full aircraft model at high reynolds numbers in the european transonic windtunnel.” *Journal of Sound and Vibration*, 2023. doi:10.1016/j.jsv.2023.117926.
- [3] C. J. Bahr, W. M. Humphreys, D. Ernst, T. Ahlefeldt, C. Spehr, A. Pereira, Q. Leclere, C. Picard, R. Porteous, D. Moreau, J. Fischer, and C. J. Doolan. “A Comparison of Microphone Phased Array Methods Applied to the Study of Airframe Noise in Wind Tunnel Testing.” In *AIAA*. Denver, United States, 2017. doi:10.2514/6.2015-2206. URL <https://hal.science/hal-01595856>.
- [4] G. Chardon. “Gridless covariance matrix fitting methods for three dimensional acoustical source localization - source code.” URL https://github.com/gilleschardon/SFWCMF/blob/main/hr_clean_sc.m.
- [5] G. Chardon. “Theoretical analysis of beamforming steering vector formulations for acoustic source localization.” *Journal of Sound and Vibration*, 517, 116544, 2022. ISSN 0022-460X. doi:10.1016/j.jsv.2021.116544.
- [6] G. Chardon. “Gridless covariance matrix fitting methods for three dimensional acoustical source localization.” *Journal of Sound and Vibration*, 551, 117608, 2023. ISSN 0022-460X. doi:<https://doi.org/10.1016/j.jsv.2023.117608>.
- [7] Y. Chi, L. L. Scharf, A. Pezeshki, and A. R. Calderbank. “Sensitivity to basis mismatch in compressed sensing.” *IEEE Transactions on Signal Processing*, 59(5), 2182–2195, 2011. doi:10.1109/tsp.2011.2112650.
- [8] E. Daniel, R. Geisler, F. Philipp, T. Ahlefeldt, A. Goudarzi, and S. Carsten. “Enhancing aeroacoustic wind tunnel studies through massive channel upscaling with mems microphones.” In *30th AIAA/CEAS Aeroacoustics Conference*. 2024.
- [9] D. Ernst. *Akustischer Kohärenzverlust in offenen Windkanälen aufgrund der turbulenten Scherschicht*. Ph.D. thesis, Technische Universität Berlin, 2020. doi:10.14279/DEPOSITONCE-9712.
- [10] A. Goudarzi. “Bebec 2024 - source code.” URL <https://github.com/ArminGoudarzi>.
- [11] A. Goudarzi. “Frequency domain beamforming using neuronal networks.” In *Berlin Beamforming Conference 2022*. 2022.
- [12] A. Goudarzi. “B-CLEAN-SC: CLEAN-SC for broadband sources.” *JASA Express Letters*, 3(9), 094804, 2023. ISSN 2691-1191. doi:10.1121/10.0020992.
- [13] A. Goudarzi. *Improving the analysis of aeroacoustic measurements through machine learning*. Ph.D. thesis, University Goettingen, 2023. doi:10.53846/goediss-10205.
- [14] A. Goudarzi. “Global, and local optimization beamforming for broadband sources.” *The Journal of the Acoustical Society of America*, 155(1), 262–273, 2024. ISSN 0001-4966. doi:10.1121/10.0024247.

- [15] A. Goudarzi, C. Spehr, and S. Herbold. “Automatic source localization and spectra generation from sparse beamforming maps.” *J. Acoust. Soc. Am.*, 150(3), 1866–1882, 2021. doi:10.1121/10.0005885.
- [16] A. Goudarzi, C. Spehr, and S. Herbold. “Expert decision support system for aeroacoustic source type identification using clustering.” *J. Acoust. Soc. Am.*, 151(2), 1259–1276, 2022. doi:10.1121/10.0009322.
- [17] J. A. Högbom and T. J. Cornwell. “Aperture synthesis with a non-regular distribution of interferometer baselines. commentary.” *Astronomy and Astrophysics*, 500, 55–66, 1974.
- [18] A. Kujawski and E. Sarradj. “Fast grid-free strength mapping of multiple sound sources from microphone array data using a transformer architecture.” *The Journal of the Acoustical Society of America*, 152(5), 2543–2556, 2022. doi:10.1121/10.0015005.
- [19] A. M. N. Malgouzar, M. Snellen, R. Merino-Martinez, D. G. Simons, and P. Sijtsma. “On the use of global optimization methods for acoustic source mapping.” *The Journal of the Acoustical Society of America*, 141(1), 453–465, 2017. doi:10.1121/1.4973915.
- [20] R. Merino-Martínez, P. Sijtsma, M. Snellen, T. Ahlefeldt, J. Antoni, C. J. Bahr, D. Blacodon, D. Ernst, A. Finez, S. Funke, T. F. Geyer, S. Haxter, G. Herold, X. Huang, W. M. Humphreys, Q. Leclère, A. Malgouzar, U. Michel, T. Padois, A. Pereira, C. Picard, E. Sarradj, H. Siller, D. G. Simons, and C. Spehr. “A review of acoustic imaging methods using phased microphone arrays.” *CEAS Aeronautical Journal*, 10(1), 197–230, 2019. ISSN 1869-5590. doi:10.1007/s13272-019-00383-4.
- [21] A. Neumaier. “Complete search in continuous global optimization and constraint satisfaction.” *Acta Numerica*, 13, 271–369, 2004. doi:10.1017/S0962492904000194.
- [22] E. Sarradj. “Three-dimensional acoustic source mapping with different beamforming steering vector formulations.” *Advances in Acoustics and Vibration*, 2012, 1–12, 2012. doi:10.1155/2012/292695.
- [23] P. Sijtsma. “CLEAN based on spatial source coherence.” *Int. J. Aeroacoustics*, 6, 357–374, 2007. doi:10.1260/147547207783359459.
- [24] P. Sijtsma, R. Merino-Martinez, A. M. Malgouzar, and M. Snellen. “High-resolution CLEAN-SC: Theory and experimental validation.” *International Journal of Aeroacoustics*, 16(4-5), 274–298, 2017. doi:10.1177/1475472x17713034.
- [25] M. Vanderveen, B. Ng, C. Papadias, and A. Paulraj. “Joint angle and delay estimation (JADE) for signals in multipath environments.” In *Conference Record of The Thirtieth Asilomar Conference on Signals, Systems and Computers*, volume 2, pages 1250–1254. IEEE Comput. Soc. Press, 1996. doi:10.1109/acssc.1996.599145.
- [26] B. von den Hoff, R. Merino-Martínez, D. G. Simons, and M. Snellen. “Using global optimization methods for three-dimensional localization and quantification of incoherent acoustic sources.” *JASA Express Letters*, 2(5), 054802, 2022. doi:10.1121/10.0010456.